Morphologies and kinetics of a dewetting ultrathin solid film

M. Khenner

Department of Mathematics, State University of New York at Buffalo, Buffalo, New York 14260, USA
(Received 11 April 2008; published 30 June 2008)

The surface evolution model based on a geometric partial differential equation is used to numerically study the kinetics of dewetting and the dynamic morphologies for the localized pinhole defect in the surface of an ultrathin solid film with the strongly anisotropic surface energy. Depending on the parameters such as the initial depth and width of the pinhole, the strength of the attractive substrate potential and the strength of the surface-energy anisotropy, the pinhole may either extend to the substrate and thus rupture the film, or evolve to the quasiequilibrium shape while the rest of the film surface undergoes a phase separation into a hill-and-valley structure followed by coarsening. Emergence of the quasiequilibrium shape and the termination of a dewetting are associated with the faceting of the pinhole tip. Overhanging (nongraph) morphologies are possible for deep, narrow (slitlike) pinholes.

I. INTRODUCTION

Recent experiments[1,2] with the sub-10-nm silicon-on-insulator films at $800-900\,^{\circ}\mathrm{C}$ demonstrate Si film dewetting. The mass transport in this system is by thermally activated surface diffusion, and there is no stress at the film-substrate interface due to an absence of a lattice mismatch between the film and the SiO_2 substrate. Dewetting starts at randomly distributed pinhole defects in the Si planar surface. The pinholes may exist prior to the annealing, or they form shortly after the temperature is raised. Conditions favoring pinhole deepening over contraction, where the latter is caused by minimization of the surface area due to the mean surface energy (tension), and the kinetics of the pinhole and its dynamic shape, are not presently known. While the physical mechanisms responsible for dewetting and agglomeration of the islands are the subject of a debate,[3] there is little doubt that the long-range film-substrate interactions (which are also called wetting interactions) provide a major driving force for dewetting in the ultrathin, single crystal semiconductor-on-insulator thin films.[4,5]

It must be noted that in contrast to liquids, the surface energy of solid surfaces is strongly anisotropic, leading to missing orientations in the dynamic or equilibrium surface shape[6–10] and faceting instability.[11–18] Anisotropy is certain to affect the dynamics of the pinhole. Moreover, it is possible that the nonlinear competition with the attractive wetting potential may even lead to the emergence of an equilibrium and thus to the suppression of the film dewetting and rupture.

In Ref. 19, following Ref. 20, the partial differential equation (PDE)-based model is developed, which allows to predict the wavelength of the fastest growing cosinelike perturbation of the film surface (also called the normal perturbation), assuming surface diffusion and the two-layer wetting potential.[20–24] The model also enables computation of the dynamical, faceted morphologies. Such computations are performed for the normal perturbation and they demonstrate the stabilizing impact of the surface-energy anisotropy on dewetting dynamics. The model can in principle support any reasonable form of the wetting potential, but the corresponding contribution to the governing PDE for the film thickness must be rederived.

In this paper, using the model of Ref. 19, the kinetics and morphologies are computed systematically for the *localized* surface defect from the full nonlinear PDE. As has been made clear above, real surface defects are necessarily localized. We compute for different widths and depths of the pinhole and, for all other model parameters fixed, observe very different dynamics and dewetting outcomes. We also relax the assumption made in Ref. 19 that the surface height above the substrate is described by a function $h(x,t)$ [i.e., a one-dimensional (1D) surface is nonoverhanging] and reformulate the model in terms of two parametric PDEs. This allows computing, say, beyond the surface-phase separation[11,12] into orientations 0° and 90° for some surface-energy anisotropies. Asymmetric morphologies and different kinetics may arise when the direction of the maximum surface energy is not the reference direction for the shape evolution (i.e., for instance, the z axis perpendicular to the substrate), which is often the case. Thus we incorporate such misorientation in the model. Note that parametric formulations of the geometric surface-evolution laws are common, see for instance Refs. 25–28.

II. PROBLEM STATEMENT

A two-dimensional (2D) film with the free one-dimensional (1D) parametric surface $\Upsilon[x(u,t),z(u,t)]$ is assumed, where x and z are the Cartesian coordinates of a point on a surface, t is time and u is the parameter along the surface. The origin of the Cartesian reference frame is on the substrate, and along the substrate (x direction, or the [10] crystalline direction) the film is assumed infinite. The z axis is along the [01] crystalline direction, which is normal to the substrate. Marker particles are used to track the surface evolution.[29] Thus x and z in fact represent the coordinates of a marker particle, which are governed by the two coupled parabolic PDEs:[25,26,30,31]

$$x_t = V\frac{1}{g}z_u, \tag{1a}$$

$$z_t = -V\frac{1}{g}x_u, \tag{1b}$$

Here the subscripts t and u denote the differentiation, V is the normal velocity of the surface, which incorporates the phys-

ics of the problem, and $g = ds/du = \sqrt{x_u^2 + z_u^2}$ is the metric function (where s is the arclength).

The normal velocity of the surface is due to gradients of the surface chemical potential μ, which drive the mass flux of adatoms along the surface. In other words, the redistribution of adatoms along the surface changes its shape, which is equivalent to the surface moving in the normal direction.[32–34] The chemical potential is the sum of two contributions, $\mu = \mu^{(\kappa)} + \mu^{(w)}$, where $\mu^{(\kappa)}$ is the regular contribution due to the surface mean curvature κ, and $\mu^{(w)}$ is the wetting chemical potential with the characteristic exponential decay:[20,23]

$$\mu^{(w)} = \Omega[\gamma_p(\theta) - \gamma_S]\frac{\exp(-z/\ell)}{\ell}\cos\theta, \quad z > 0. \quad (2)$$

Here Ω is the atomic volume, θ is the angle that the unit surface normal makes with the [01] crystalline direction, $\gamma_S = \text{const.}$ is the surface energy of the substrate in the absence of the film, ℓ is the characteristic wetting length, and $\gamma_p(\theta)$ is the primary part of the anisotropic surface energy of the film, i.e., for typical fourfold anisotropy

$$\gamma(\theta) = \gamma_0[1 + \epsilon_\gamma \cos 4(\theta + \beta)] + \frac{\delta}{2}\kappa^2 \equiv \gamma_p(\theta) + \frac{\delta}{2}\kappa^2. \quad (3)$$

In Eq. (3) γ_0 is the mean value of the surface energy, ϵ_γ determines the degree of anisotropy, β is the misorientation angle, and δ is the small non-negative regularization parameter having units of energy. The δ term in Eq. (3) makes the evolution [Eqs. (1a) and (1b)] mathematically well posed for strong anisotropy.[11,12,14,35–37] (The anisotropy is weak when $0 < \epsilon_\gamma < 1/15$ and strong when $\epsilon_\gamma \geq 1/15$. $\delta = 0$ in the former case.) The surface energy has a maximum at $4(\theta + \beta) = 0$, i.e., at $\theta = -\beta$. For $\beta = 0$, this direction is the z axis.

The curvature contribution to μ is[19,20,23]

$$\mu^{(\kappa)} = \Omega\left[\left(\gamma_p + \frac{\partial^2\gamma_p}{\partial\theta^2}\right)(1 - \exp(-z/\ell))\kappa + \gamma_S\exp(-z/\ell)\kappa \right.$$
$$\left. - \frac{\delta}{\gamma_0}\left(\frac{\kappa^3}{2} + \kappa_{ss}\right)\right], \quad (4)$$

where the subscript s denotes the differentiation with respect to the arclength. If the wetting potential is zero ($z/\ell \to \infty$), this reduces to the familiar strongly anisotropic form.[11,12,14]

Finally,

$$\kappa = g^{-3}(z_{uu}x_u - x_{uu}z_u) \quad (5)$$

and

$$V = \frac{D\nu}{kT}[\mu_{ss}^{(\kappa)} + \mu_{ss}^{(w)}], \quad (6)$$

where D is the adatoms diffusivity, ν is the adatoms surface density, k is the Boltzmann constant, and T is the absolute temperature. The only differences of this formulation from the formulation in Ref. 19, except for accounting for the surface energy misorientation in Eq. (3) and the parametric representation, are that in Eq. (4) the wetting (exponential)

contributions are accounted for in full (that is, the approximation in the form of averaging across the film thickness is not employed), and the regularization term is not included in $\mu^{(w)}$. ($\mu^{(w)}$ does not contain the surface stiffness $\gamma + \gamma_{\theta\theta}$ and thus it does not make the PDE ill-posed for strong anisotropy. Besides, the regularization contribution to $\mu^{(w)}$ is vanishingly small for large surface slopes due to its proportionality to h_x^{-7}, see Ref. 19).

To nondimensionalize the problem, the thickness of the planar undisturbed film, h_0, is chosen as the length scale, and h_0^2/D as the time scale. Also, let $r = \ell/h_0$. The dimensionless problem is comprised of Eqs. (1a), (1b), and (5) (where the differentiations are with respect to the dimensionless variables), and where

$$V = B[\mu_{ss}^{(\kappa)} + \mu_{ss}^{(w)}], \quad (7a)$$

$$\mu^{(\kappa)} = \left(\gamma_p + \frac{\partial^2\gamma_p}{\partial\theta^2}\right)[1 - \exp(-z/r)]\kappa$$
$$+ \Gamma\exp(-z/r)\kappa - \Delta\left(\frac{\kappa^3}{2} + \kappa_{ss}\right), \quad (7b)$$

$$\mu^{(w)} = [\gamma_p(\theta) - \Gamma]\frac{\exp(-z/r)}{r}\cos\theta, \quad (7c)$$

$$\gamma_p(\theta) = 1 + \epsilon_\gamma\cos 4(\theta + \beta), \quad (7d)$$

$$\cos\theta = \frac{z_u}{g}. \quad (7e)$$

In Eqs. (7a)–(7e), $B = \Omega^2\nu\gamma_0/(kTh_0^2)$, $\Gamma = \gamma_S/\gamma_0$, and $\Delta = \delta/(\gamma_0 h_0^2)$. For the computational method, using the relation between s and u,

$$\frac{\partial}{\partial s} = \frac{1}{g}\frac{\partial}{\partial u}, \quad (8)$$

the problem is written entirely in terms of the independent variables u and t (not shown).

In the simulations reported below, the following values of the physical parameters are used: $D = 1.5 \times 10^{-6}$ cm^2/s, $\Omega = 2 \times 10^{-23}$ cm^3, $\gamma_0 = 10^3$ erg/cm^2, $\gamma_S = 5 \times 10^2$ erg/cm^2, $\nu = 10^{15}$ cm^{-2}, $kT = 1.12 \times 10^{-13}$ erg, $h_0 = 10^{-6}$ cm, and $\delta = 5 \times 10^{-12}$ erg. These values translate into $B = 3.57 \times 10^{-3}$, $\Gamma = 0.5$, and $\Delta = 5 \times 10^{-3}$. In this paper we consider strong anisotropy, $\epsilon_\gamma > 1/15$. Also, $r = 0.02, 0.1$.

The initial condition in all simulations is the Gaussian surface

$$z(x,0) = 1 - d\exp\left[-\left(\frac{x-5}{w}\right)^2\right], \quad 0 \leq x \leq 10 \quad (9)$$

where $0 < d < 1$ and w are the depth and the "width" of the pinhole at $t = 0$, respectively (see Fig. 4). The length of the computational domain equals to ten times the unperturbed film thickness, and the defect is positioned at the center of the domain. We use values $d = 0.5, 0.9$, which correspond to the shallow and the deep pinhole at $t = 0$, respectively, and
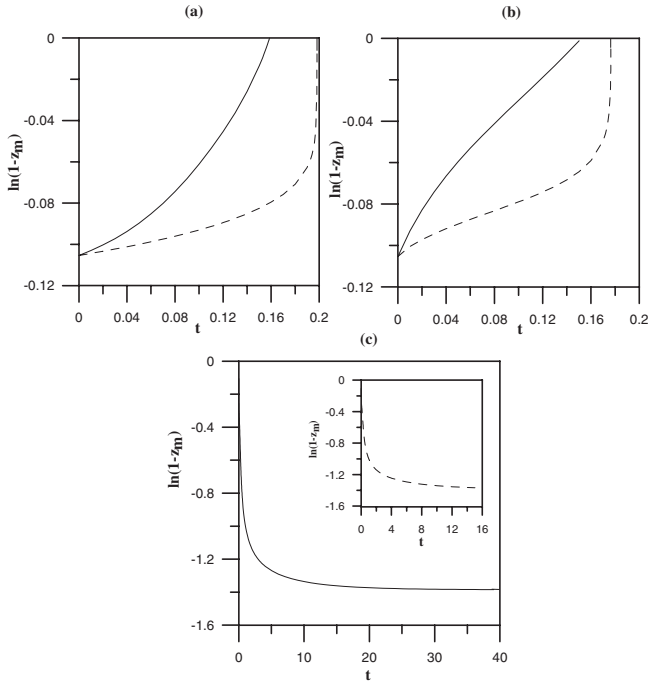
FIG. 1. Kinetics (rate) data for the deep pinhole ($d=0.9$). $\epsilon_\gamma=1/12$, $\beta=0$. Line slope equals the rate of the tip evolution. Solid line: $r=0.1$. Dash line: $r=0.02$. (a) Wide pinhole ($w=2$). (b) Intermediate pinhole ($w=1$). (c) Narrow pinhole ($w=0.15$).

$w=0.15$ (the narrow pinhole), $w=1$ (the intermediate pinhole), and $w=2$ (the wide pinhole).

The method of lines is used for the computation with the periodic boundary conditions at $x=0,10$. Equations (1a) and (1b) are discretized by second-order finite differences on a spatially uniform grid in u. The integration in time of the resulting coupled system of the nonlinear ordinary differential equations is done using the implicit Runge-Kutta method of the Radau family.[38] Initially $u \equiv x$, but periodically (usually after every few tens of the time steps) the marker particles are positioned at the nodes of the uniform grid in s, and the surface is reparametrized so that u becomes the arclength. [Note that Eqs. (1a) and (1b) are reparametrization invariant.[25]] This is done through fitting the surface by an interpolatory, parametric cubic spline curve, in order to prevent the marker particles from coming too close or too far apart in the course of the surface evolution.[39] Between the calls to the reparametrization routine, the arclength is changing as the surface evolves, but the grid spacing in u is constant and equal to the last computed arclength spacing.

III. RESULTS

A. Kinetics

Figures 1 and 2 show the log-normal plots of the pinhole depth vs time, for $d=0.9$ and $d=0.5$, respectively. z_m is the height of the surface at the tip of the pinhole.

Wide and intermediate deep pinholes dewet but the depth of the narrow deep pinhole decreases until it reaches quasiequilibrium at $z=0.75$ (Fig. 1). Quasiequilibrium means that z_m (or, equivalently, the depth) changes very slowly or not at
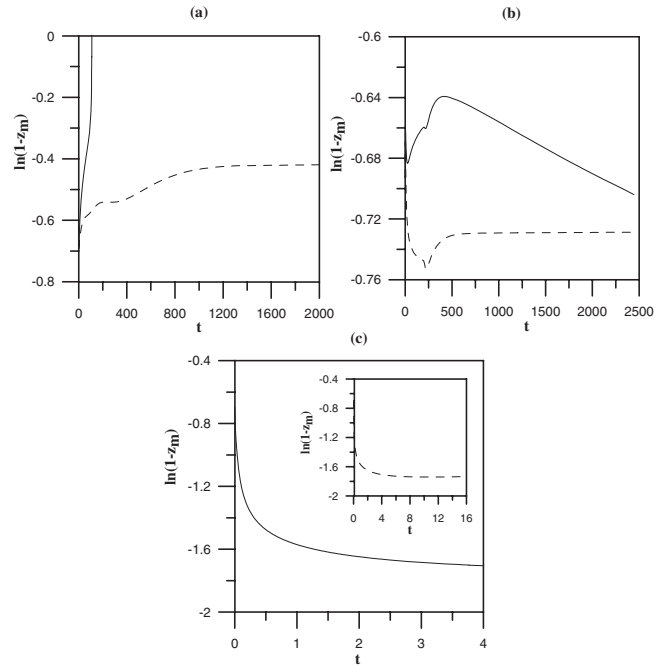

FIG. 2. Same as Fig. 1, but for the shallow pinhole ($d=0.5$).

all, while the rest of the shape may change relatively fast. Correspondingly, we will call the surface shape at the time when the quasiequilibrium depth is attained the quasiequilibrium shape. [Again, this shape *is* changing, but the height of its minimum point (the tip) is not changing, or is changing very slowly.] Also notice in Figs. 1(a) and 1(b) that the growth rate at the rupture time is finite for $r=0.1$ but infinite (or extremely large) for $r=0.02$, and the time to rupture is somewhat less for $r=0.1$. However, from Fig. 1(c), the time to reach quasiequilibrium is about ten times larger for $r=0.1$ than for $r=0.02$.

As can be seen in Fig. 2, only the wide shallow pinhole dewets, and only when $r=0.1$. In all other cases of w and r (except $w=1$, $r=0.1$, shown by the solid line in Fig. 2(b)) the quasiequilibrium is achieved. For $w=1$, $r=0.1$, the depth is initially a non-monotonic function of time, but after the transient phase it monotonically and slowly decreases without reaching the quasiequilibrium (we computed for $t \leq 2 \times 10^4$). Also, one can see that for $r=0.02$ the depth at quasiequilibrium decreases as w decreases, and it takes less time to reach quasiequilibrium as w decreases.

In Fig. 3 the dewetting kinetics is compared for several misorientations and strengths of the anisotropy. Shown in the said figure is the case of the deep, wide pinhole and $r=0.1$. The time to rupture increases insignificantly with the decrease in anisotropy or with the increase in the misorientation angle. The faster dewetting for stronger anisotropy here can be attributed to the initial faster shape changes due to larger gradients of $\mu^{(\kappa)}$, i.e., before the surface orientation falls into an unstable (spinodal) range and faceting intervenes, and to the proximity of the pinhole tip to the substrate. That the misorientation slows the kinetics is well known; for instance Liu & Metiu[11] in their important study of faceting call the similar situation an "off-critical quench," and find that at sufficiently large misorientations the "crystal surface
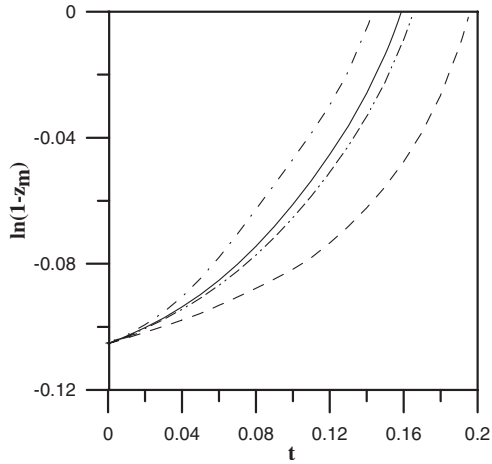
FIG. 3. Kinetics data for the deep, wide pinhole. $r=0.1$. Solid line: $\epsilon_\gamma=1/12$, $\beta=0$. Dash line: $\epsilon_\gamma=1/12$, $\beta=10°$. Dash-dot line: $\epsilon_\gamma=1/8$, $\beta=0$. Dash-dash-dot-dot line: $\epsilon_\gamma=1/14$, $\beta=0$.

will not phase-separate *spontaneously*, but will have to overcome a finite free-energy barrier."

B. Morphologies

Figure 4 shows the initial and the final surface shapes of the initially deep pinhole for the three values of w. The kinetics of the corresponding *dynamical* shapes is shown in Figs. 1(a)–1(c) by solid lines and has been discussed above. Dewetting of the wide and intermediate pinholes proceeds through the extension of the tip of the pinhole until it reaches the substrate at 57°. The quasiequilibrium shape for the narrow pinhole is very similar to the one shown in Fig. 6(c). The
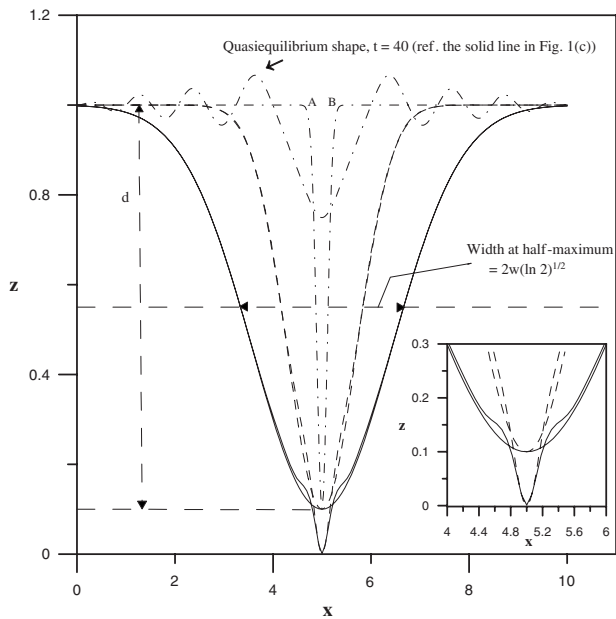

FIG. 4. Surface morphologies for the deep pinhole. $r=0.1$, $\epsilon_\gamma=1/12$, $\beta=0$. The depth (d) and the width (w) of the pinhole at $t=0$ are defined. Solid, dash, dash-dot line: $w=2,1,0.15$, respectively. Inset: the magnified view of the dewetting region for $w=2,1$.

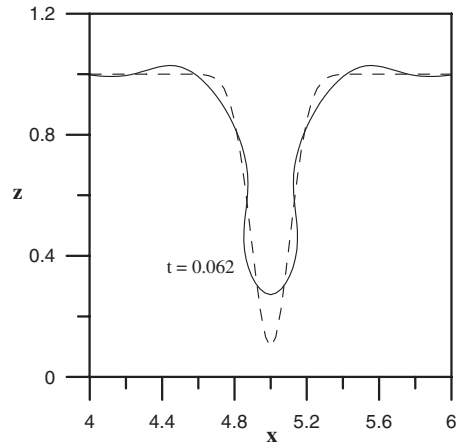
FIG. 5. Magnified view of the transient, overhanging surface morphology for the deep, narrow pinhole from Fig. 4. Dash line: the surface at $t=0$.

latter shape is discussed in more details below. While evolving from the initial slitlike shape to the quasiequilibrium shape, the surface of the narrow pinhole overhangs (Fig. 5), until it slowly returns to the nonoverhanging shape later. In the time interval where the overhanging takes place, the surface slope is large and nonanalytic.

Surface shapes for the initially shallow pinhole are shown in Fig. 6. Characteristic of these shapes is an emergence of the hill-and-valley structure,[8] which becomes possible even when the film dewets [case of the wide pinhole in Fig. 6(a)]
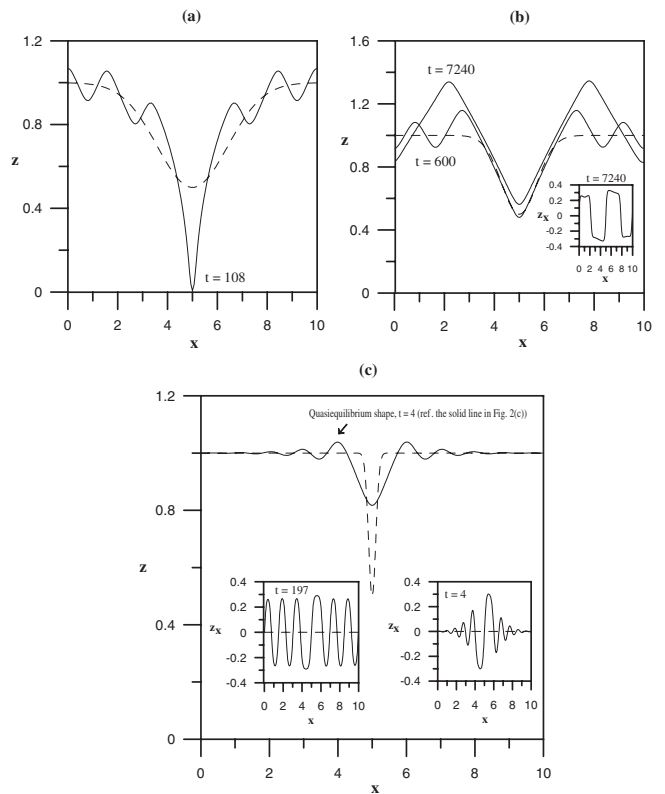

FIG. 6. Surface morphologies for the shallow pinhole. $r=0.1$, $\epsilon_\gamma=1/12$, $\beta=0$. (a): $w=2$, (b): $w=1$, (c): $w=0.15$. Dash line: the surface at $t=0$.
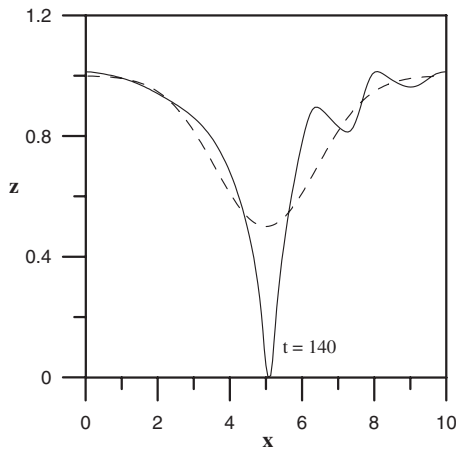
FIG. 7. Surface morphology for the shallow, wide pinhole. $r=0.1$, $\epsilon_\gamma=1/12$, $\beta=10°$. Dash line: the surface at $t=0$.

due to the larger time required to reach the substrate in this case. The angle at rupture is 90°. Figure 6(b) shows coarsening of the structure for the intermediate-width case. As has been pointed out above at the discussion of Fig. 2(b), in this case there is no quasiequilibrium (at least for $t \leq 2 \times 10^4$), and the tip recedes toward the unperturbed height $h=1$. Note that the apparent recession rate is slower than the overall coarsening rate. $t=7240$ is the time when the two pyramidal structures appear on the film surface. The slope of their walls is shown in the inset, and it is almost constant in each of the four characteristic intervals of x, with each interval corresponding to a facet. For $7240 < t \leq 2 \times 10^4$ the walls (facets) become more straight, and the graph of $z_x(x)$ becomes nearly constant in each of the four characteristic intervals. Figure 6(c) shows the quasiequilibrium shape for the narrow pinhole. Formation of the hill-and-valley structure followed by coarsening continues for $t > 4$, as is evidenced by the surface slope shown in the inset at the left, but the pinhole depth at $x=5$ is constant. (In fact, the difference of depths at $t=197$ and at $t=4$ is 0.007.) Note that the formation of the hill-and-valley structure, its coarsening, and slope selection have been the subject of many papers, see for instance Refs. 5, 11–18, 20, 21, 23, and 40–46. (Refs. 20, 21, and 23 discuss the impacts of wetting interactions.) Since in this paper we are interested in characterizing dewetting and rupture, we do not further pursue that direction.

Finally, Fig. 7 demonstrates impacts of the misorientation ($\beta=10°$) on morphology. As expected, asymmetrical shapes emerge for $\beta \neq 0°$. While the wide, shallow pinhole dewets, only its right sidewall undergoes the phase separation into a hill-and-valley structure. Kinetics is very similar to the case $\beta=0$, see Fig. 2(a) (solid line).

IV. DISCUSSION

In this paper a fully nonlinear model is used to compute the complex scenarios of dewetting/equilibration for a localized pinhole defect in the surface of a strongly anisotropic thin solid film, assuming the two-layer, exponentially decaying wetting potential and zero lattice mismatch with the substrate.
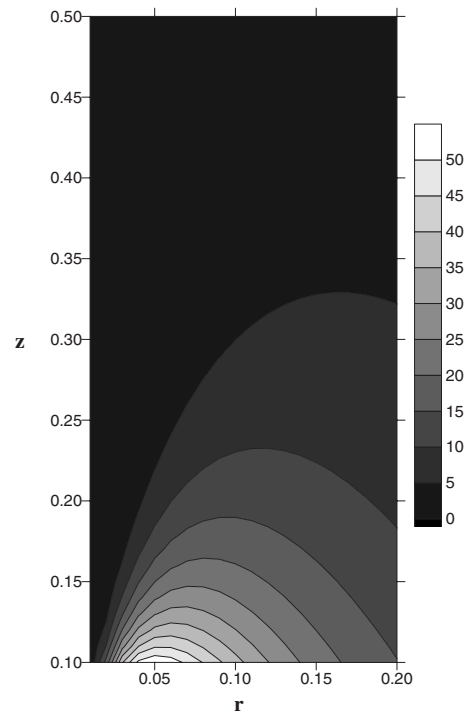

FIG. 8. Contour plot of the dewetting factor $\exp(-z/r)/r^2$.

The computed dewetting kinetics can be explained at large using the magnitude of the dewetting factor. In Ref. 19 it was shown that the dominant dewetting terms in the mass-conservation evolution PDE are proportional to $\exp(-z/r)/r^2$ (for $r<1$). This is plotted in Fig. 8. One can see that for $r=0.1, 0.02$ the maximum of this factor occurs for the small values of the film thickness. This explains why all but one initial conditions in Fig. 1 (deep pinhole) lead to the pinhole-depth increase until the film dewets, while all but one initial conditions in Fig. 2 (shallow pinhole) lead to the decrease of the pinhole depth. In other words, quite naturally the dewetting is more promoted for larger values of the dewetting factor. The dewetting factor can also explain the small (large) difference in the characteristic time scales for $r=0.1$ and $r=0.02$ in Fig. 1(a) [Fig. 2(a)]. Indeed, for the case of Fig. 1(a) the factor is 36.8 ($r=0.1$) and 16.8 ($r=0.02$) vs, respectively, 0.7 and 3×10^{-8} for the case of Fig. 2(a). Evolution of the film also depends strongly on the film shape and whether θ is in the unstable range. When it is, as in the cases shown in Figs. 4–7 then, the faceting instability is energetically more favorable than dewetting, and most often the competition of the two processes causes the unusual hill-and-valley structure, where a shallow pinhole remains despite the structure coarsening (which takes place separately at the both shoulders of the pinhole). Note that the faceting instability seems to be always initiated where the surface changes from the horizontal to a sidewall (regions A and B in Fig. 4).

We also point out that in our computations, the pinhole tip is always nonfaceted at rupture [see Figs. 4, 6(a), and 7]. In fact, dewetting ceases if the facet spreads to the tip. This is observed in the evolution of the intermediate, shallow pinhole [Figs. 2(b) and 6(b)]. Also, if the pinhole is not too deep (Fig. 4), then the contact angle with the substrate at rupture is 90°. In reality, after the contact this value changes in order to

minimize the total energy of the surface-substrate system. For instance, for the silicon-on-insulator the measured and the calculated values of the equilibrium contact angle coincide (73°).[1,3]

[1] B. Yang, P. Zhang, D. E. Savage, M. G. Lagally, G.-H. Lu, M. Huang, and F. Liu, Phys. Rev. B **72**, 235413 (2005).

[2] P. Sutter, W. Ernst, Y. S. Choi, and E. Sutter, Appl. Phys. Lett. **88**, 141924 (2006).

[3] D. T. Danielson, D. K. Sparacin, J. Michel, and L. C. Kimerling, J. Appl. Phys. **100**, 083507 (2006).

[4] Z. Suo and Z. Zhang, Phys. Rev. B **58**, 5116 (1998).

[5] C.-h. Chiu, Phys. Rev. B **69**, 165413 (2004).

[6] G. Wulff, Z. Kristallogr. **34**, 449 (1901).

[7] C. Herring, in *Structure and Properties of Solid Surfaces*, edited by R. Gomer and C. S. Smith (University Chicago Press, Chicago, 1953), pp. 5–81.

[8] C. Herring, Phys. Rev. **82**, 87 (1951).

[9] H. P. Bonzel and E. Preuss, Surf. Sci. **336**, 209 (1995).

[10] H. P. Bonzel, Phys. Rep. **385**, 1 (2003).

[11] F. Liu and H. Metiu, Phys. Rev. B **48**, 5808 (1993).

[12] J. Stewart and N. Goldenfeld, Phys. Rev. A **46**, 6505 (1992).

[13] D. G. Vlachos, L. D. Schmidt, and R. Aris, Phys. Rev. B **47**, 4896 (1993).

[14] A. A. Golovin, S. H. Davis, and A. A. Nepomnyashchy, Physica D **122**, 202 (1998).

[15] A. A. Golovin, S. H. Davis, and A. A. Nepomnyashchy, Phys. Rev. E **59**, 803 (1999).

[16] T. V. Savina, A. A. Golovin, S. H. Davis, A. A. Nepomnyashchy, and P. W. Voorhees, Phys. Rev. E **67**, 021606 (2003).

[17] J. J. Eggleston, G. B. McFadden, and P. W. Voorhees, Physica D **150**, 91 (2001).

[18] S. J. Watson, F. Otto, B. Y. Rubinstein, and S. H. Davis, Physica D **178**, 127 (2003).

[19] M. Khenner, Phys. Rev. B **77**, 165414 (2008).

[20] A. A. Golovin, M. S. Levine, T. V. Savina, and S. H. Davis, Phys. Rev. B **70**, 235342 (2004).

[21] M. Ortiz, E. A. Repetto, and H. Si, J. Mech. Phys. Solids **47**, 697 (1999).

[22] C.-h. Chiu and H. Gao, in *Thin Films: Stresses and Mechanical Properties V*, MRS Symposia Proceedings No. 356, edited by S. P. Baker (Materials Research Society, Pittsburgh, 1995), p. 33.

[23] M. S. Levine, A. A. Golovin, S. H. Davis, and P. W. Voorhees, Phys. Rev. B **75**, 205312 (2007).

[24] B. J. Spencer, Phys. Rev. B **59**, 2011 (1999).

[25] R. C. Brower, D. A. Kessler, J. Koplik, and H. Levine, Phys. Rev. A **29**, 1335 (1984).

[26] T. Y. Hou, J. S. Lowengrub, and M. J. Shelley, J. Comput. Phys. **114**, 312 (1994).

[27] M. Khenner, R. J. Braun, and M. G. Mauk, J. Cryst. Growth **235**, 425 (2002); **241**, 330 (2002).

[28] M. Khenner, Comput. Mater. Sci. **32**, 203 (2005).

[29] G. Tryggvason, B. Bunner, A. Esmaeeli, D. Juric, N. Al-Rawahi, W. Tauber, J. Han, S. Nas, and Y.-J. Jan, J. Comput. Phys. **169**, 708 (2001).

[30] J. A. Sethian, Commun. Math. Phys. **101**, 487 (1985).

[31] J. A. Sethian, J. Diff. Geom. **31**, 131 (1989).

[32] W. W. Mullins, J. Appl. Phys. **28**, 333 (1957); **30**, 77 (1959).

[33] W. W. Mullins, in *Metal Surfaces* (American Society for Metals, Metals Park, OH, 1963), p. 1766.

[34] J. W. Cahn and J. E. Taylor, Acta Metall. Mater. **42**, 1045 (1994).

[35] S. Angenent and M. E. Gurtin, Arch. Ration. Mech. Anal. **108**, 323 (1989).

[36] A. Di Carlo, M. E. Gurtin, and P. Podio-Guidugli, SIAM J. Appl. Math. **52**, 1111 (1992).

[37] B. J. Spencer, Phys. Rev. E **69**, 011603 (2004).

[38] E. Hairer and G. Wanner, J. Comput. Appl. Math. **111**, 93 (1999).

[39] R. J. Renka, ACM Trans. Math. Softw. **19**, 81 (1993).

[40] M. Siegert and M. Plischke, Phys. Rev. Lett. **73**, 1517 (1994).

[41] M. Rost and J. Krug, Phys. Rev. E **55**, 3952 (1997).

[42] M. Siegert, Physica A **239**, 420 (1997).

[43] P. Politi, Phys. Rev. E **58**, 281 (1998).

[44] M. F. Gyure, J. J. Zinck, C. Ratsch, and D. D. Vvedensky, Phys. Rev. Lett. **81**, 4931 (1998).

[45] D. Moldovan and L. Golubovic, Phys. Rev. E **61**, 6190 (2000).

[46] R. V. Kohn, Commun. Pure Appl. Math. **56**, 1549 (2003).